RESEARCH PAPER

EXPLORING THE ROLE OF LAND USE SETTINGS ON LANDSLIDE ELLIPTICITY IN VOLCANIC FOOT SLOPE OF THE SOUTHERN SUMBING MOUNTAIN, CENTRAL-JAVA INDONESIA

Rina Purwaningsih[1,4], Junun Sartohadi[2,4*], Guruh Samodra[3], Christopher Gomez[5]
[1]Department of Environmental Science, Universitas Gadjah Mada, Yogyakarta, 55281, Indonesia
[2]Department of Soil Science, Universitas Gadjah Mada, Yogyakarta, 55281, Indonesia
[3]Department of Environmental Geography, Universitas Gadjah Mada, Yogyakarta, 55281, Indonesia
[4]Research Center of Land Resource Management, Universitas Gadjah Mada, Yogyakarta, 55281, Indonesia
[5]Faculty of Maritime Science, 5-1-1 Fukaeminami-machi Higashinada-ku, 658-0022 Kobe, Japan
***Corresponding author:** junun@ugm.ac.id
Received: March 20th 2025 / Accepted: January 27th 2026 / Published: March 31st 2026
https://doi.org/10.24057/2071-9388-2026-3962

ABSTRACT. This study investigates the effects of landslide processes on land morphology and their management strategies. Land use types determine the size and morphology of the landslide, which is critical for assessment and planning. LiDAR imaging helps to locate the various features of a landslide and human intervention. The research measures the ellipticity of landslides for a 3.2 km^2 area using LiDAR-derived data and ellipse numerical modeling. Landslide boundaries were delineated through automated and manual techniques, considering topographical index, visual interpretation, and expert knowledge. Convex hulls were used to approximate landslide shapes, which were then used to calculate the various ellipticity indices (e_L). Bare land, mixed gardens, rain-fed rice fields, and intermittent rivers have a higher e_L. Local roads, houses, and irrigated rice fields indicated receding e_L values due to the increased level of land management. Changes in eL are affected by the intensity of land use and disturbances related to the wetting of landslide slip areas. Higher ellipticity indicates dynamics in the landslide activity. Therefore, land use planning should be performed considering both natural and non-natural elements in the area.

KEYWORDS: landslide boundary shape, ellipticity index, land use settings

CITATION: Purwaningsih R., Sartohadi J., Samodra G., Gomez C. (2026). Exploring The Role Of Land Use Settings On Landslide Ellipticity In Volcanic Foot Slope Of The Southern Sumbing Mountain, Central-Java Indonesia. Geography, Environment, Sustainability, 1 (19), 72-85
https://doi.org/10.24057/2071-9388-2026-3962

Conflict of interests: The authors reported no potential conflict of interests.

INTRODUCTION

Landslides are ubiquitous geomorphic processes shaping the Earth's surface, continuously modifying landscapes through erosion and deposition (Jin et al. 2021; Pudasaini and Krautblatter 2021). These mass movements follow fundamental geomorphological principles where processes observed in the past continue into the present and future, albeit with decreasing intensity over time (Hooke, 2020). The principle of dynamic equilibrium in geomorphology suggests that landscape features evolve through a balance between erosive and depositional forces (Thorn and Welford 1994). In landslide-prone areas, this balance is particularly evident in how slope morphology changes over time. Rainwater plays a crucial role in this process, creating distinct patterns: diffusive spread in residual zones leading to convex slopes, and concentrated erosive flow in upper and middle slopes resulting in concave formations (Chen et al. 2014).

Recent studies have revealed that landslides typically create elliptical patterns in two-dimensional representations (Liu et al. 2023; Taylor et al. 2018). This geometric characteristic has become an important marker for understanding landslide behavior and evolution (Yin et al. 2014). Deviations from this elliptical pattern often indicate external influences, such as flow paths, channel morphology, or the merger of multiple smaller landslides (Martel 2004). The symmetry of these patterns can be classified into two main categories: symmetrical forms occurring on flat surfaces and asymmetrical forms on curved surfaces, each providing insight into the underlying landslide mechanics (Ogita et al. 2017).

However, human activities increasingly influence these natural patterns. Consequently, anthropogenic modifications of land cover significantly and increasingly affect landslide dynamics and susceptibility (Tarolli and Sofia 2016). Different land use types - from the broad spectrum of forest vegetation to urban development - create varying conditions for slope stability. Natural vegetation can help prevent soil erosion through root systems and reduced surface runoff, while urban expansion and agricultural development can increase landslide risks by altering drainage patterns and soil structure

(Chen et al. 2019). The relationship between land use changes and landslide morphology remains particularly important in regions experiencing rapid development. Engineering practices, construction activities, and changes in vegetation cover can substantially alter both the likelihood and characteristics of landslides. These modifications often occur without adequate risk assessment or mitigation measures, leading to increased vulnerability in previously stable areas.

Recent empirical observations suggest that while new landslides typically create elliptical scars, not all landslide boundaries maintain this shape over time (Fang et al. 2024; Li et al. 2022). The transformation of these boundaries may be influenced by both natural processes and land management practices. Understanding these changes is crucial for effective land use planning and risk mitigation in landslide-prone areas. This study aims to quantify these relationships by analyzing the ellipticity index of past and current landslide sequences in a volcanic-structural transition landscape. Specifically, we investigate how land use management influences landslide morphology, seeking to distinguish between changes caused by natural landslide processes and those resulting from anthropogenic modifications. This understanding is essential for developing more effective land management strategies in landslide-susceptible regions.

MATERIALS AND METHODS

Study Area

This research was conducted at the base of Mount Sumbing's volcanic slopes in Central Java, Indonesia (Fig. 1a). The study site exhibited distinctive pedogeological characteristics, as shown in Fig. 1b, with tertiary volcanic subsurface materials influencing quaternary volcanic surface materials. Bedrock is dominated by andesitic volcanic breccias and reworked volcanic sediments that have undergone intense hydrothermal alteration, producing clay-rich mineral assemblages dominated by kaolinite, halloysite, illite, and abundant quartz (Noviyanto et al. 2020; Purwaningsih et al. 2025). These processes have resulted in steep slopes mantled by a thick debris and soil cover, generally exceeding 80–120 cm, formed from volcanic ash deposition and prolonged weathering (Pratiwi et al. 2019). These unique pedogeological features have produced steep slopes mantled by substantial soil depth composed of clay-rich, deeply weathered materials.

The thick soil in the research area, formed through volcanic ash deposition, was also influenced by Tertiary hydrothermal alteration processes (Noviyanto et al. 2020; Pulungan and Sartohadi 2018; Samodra et al. 2020). The hydrothermal alteration of Tertiary breccia rocks produced weathered material with remarkably high clay content (Pirajno 2009). When exposed to water, this clay-rich weathered material became highly saturated, becoming the primary factor contributing to landslides (Wida et al. 2019).

Landslides occurred in areas with thick, uniform soil material, creating distinctive surface features at the research site. The concave and convex surface features observed in the hillshade image of the study site (Fig. 1c) suggest evidence of past landslide activity. This soil type was characterized by its consistent texture and composition and was prone to waterlogging (Wida et al. 2019). Water saturation reduced frictional resistance along the surface, increasing the likelihood of collapse. Water infiltration increased pore water pressure, reducing soil shear strength and facilitating slippage. The combination of uniform soil structure and high-water content created conditions where soil masses underwent rotational movement around a well-defined axis, resulting in rotational landslides. In two dimensions, these rotational landslides appeared as elliptical shapes.

The site's land use history and evolution were carefully examined, as human activities can significantly affect slope stability, influencing landslide susceptibility and associated hazards (Fell et al. 2008). This anthropogenic transformation is common across various global regions, creating localized impacts known as "local geomorphic change" (Bruschi et al. 2013). Incorporating geomorphological information into land use planning is essential for risk zoning at both intermediate and advanced levels. Advanced hazard and risk zoning requires a comprehensive approach, including detailed mapping of geomorphological features at larger scales for site-specific assessments. For such detailed analyses, the recommended mapping scale exceeds 1:5000 (Fell et al. 2008).

This site was selected as a particular research location because it represents a unique geomorphological setting where multiple geological and climatic factors converge to influence slope instability. The combination of undulating-steep topography deeply weathered volcanic soils, and a history of hydrothermal alteration provides ideal conditions to study the triggering mechanisms and morphological expression of rotational landslides. Moreover, the area is representative of many densely populated volcanic landscapes in Indonesia, making it a strategic location for developing site-specific hazard assessment frameworks with broader applicability to similar environments.

Acquisition of Landslide Boundary Data

A Da-Jiang Innovations (DJI) Matrice 300 Aircraft, mounted with a DJI Zenmuse L1 laser sensor and a camera, recorded the landslide and its boundaries with high accuracy over the 3.2 km^2 area. DJI Zenmuse L1 has a vertical accuracy of ±3 cm; however, the actual measurement accuracy of the LiDAR data in the study area was 0.35 meters, as determined through Global Navigation Satellite System (GNSS) measurements at six control points (Fig. 2). Besides that, the aerial photos have a resolution of 5 cm. Ground control points (GCP) and benchmarks were determined via GNSS to enable precise data acquisition. Furthermore, point cloud filtering and intensity modeling were undertaken during post-processing, resulting in about 26 points/m^2 of ground point density. A Digital Terrain Model (DTM) with 0.5-meter resolution was generated for the study area, and landslide identification was used to assess the chronology of the first occurrence.

Land use and land cover (LULC) data were derived from orthophotos acquired through aerial photography in April 2023, conducted concurrently with DTM–LiDAR data collection. The simultaneous acquisition enabled manual delineation of nine LULC categories using on-screen digitizing based on standard visual interpretation elements, including color, texture, shape, size, pattern, shadow, and contextual association. The interpreted LULC map was subsequently verified through field validation.

DTM products derived from LiDAR are visualized using hillshade and Topographic Position Index (TPI) features (Fig. 3). Hillshade provides a visual representation of terrain morphology, emphasizing differences between convex and concave surfaces such as ridgelines, valleys, steep slopes, and terraces (Trantham 2023). The light–dark patterns in hillshade imagery often reveal evidence of mass movements (landslides), including scarps, translational zones, and depositional areas. TPI enhances local morphological interpretation, where positive values indicate ridges and negative values represent depressions

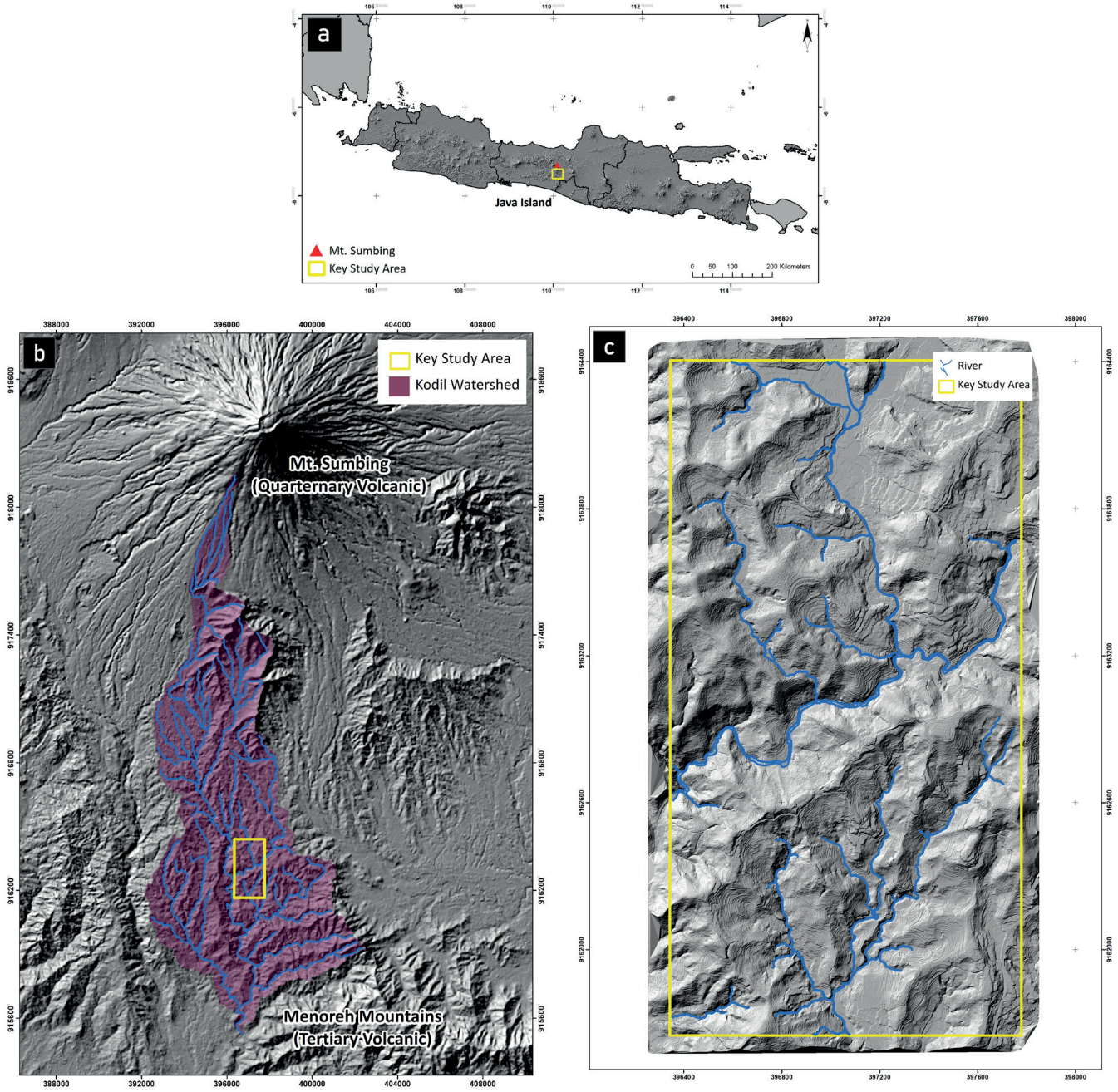

Fig. 1. Location of the Study (a) Java Island, (b) study location located between Mt. Sumbing and Menoreh Mountains, (c) Key research locations

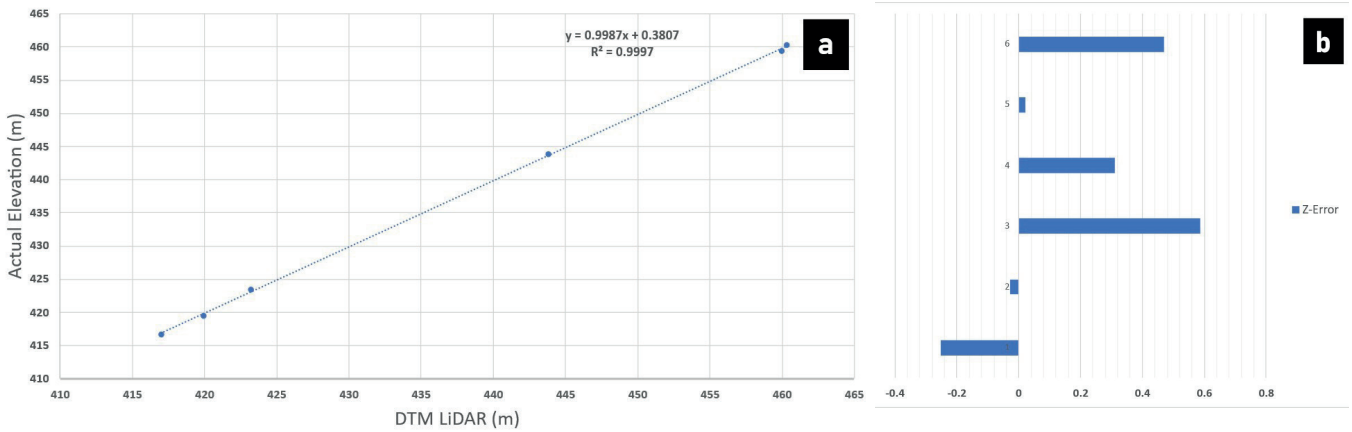

Fig. 2. (a) Linear fitting function between GNSS checkpoint elevations and DTM elevations obtained with 6 GCPs; (b) the error value represents the difference between actual and LiDAR-derived elevations

(Otgonbayar et al. 2023). In object-based analysis or terrain segmentation, hillshade and TPI support the delineation of landslide boundaries through visual interpretation.

Landslide 2D Geometrical Features and Ellipticity Identification

The elliptical descriptor developed by Schmittbuhl et al. (2003) and Tort (2003) allowed the measurement of shape, regardless of its complexity, and facilitated the conversion of morphological variations into basic geometric concepts. This procedure was challenging to perform using traditional Fourier coefficients. The Elliptical Descriptor methodology was also employed to effectively analyze the morphology of lakes, providing a robust means of describing variations and patterns between their outlines (Dhingra et al. 2019). Their synthetic morphology example confirmed that methods normalized for size and rotation were effective in grouping comparable outlines.

In this research, each delineated landslide polygon underwent ellipse numerical simulations using the methodology proposed by Taylor et al. (2018) to determine the dimensional characteristics of the landslide shapes. Computations were performed on each polygon corresponding to a landslide to determine its area (A_L), perimeter (P_L), central coordinates (x, y), and primary angle (Fig. 4).

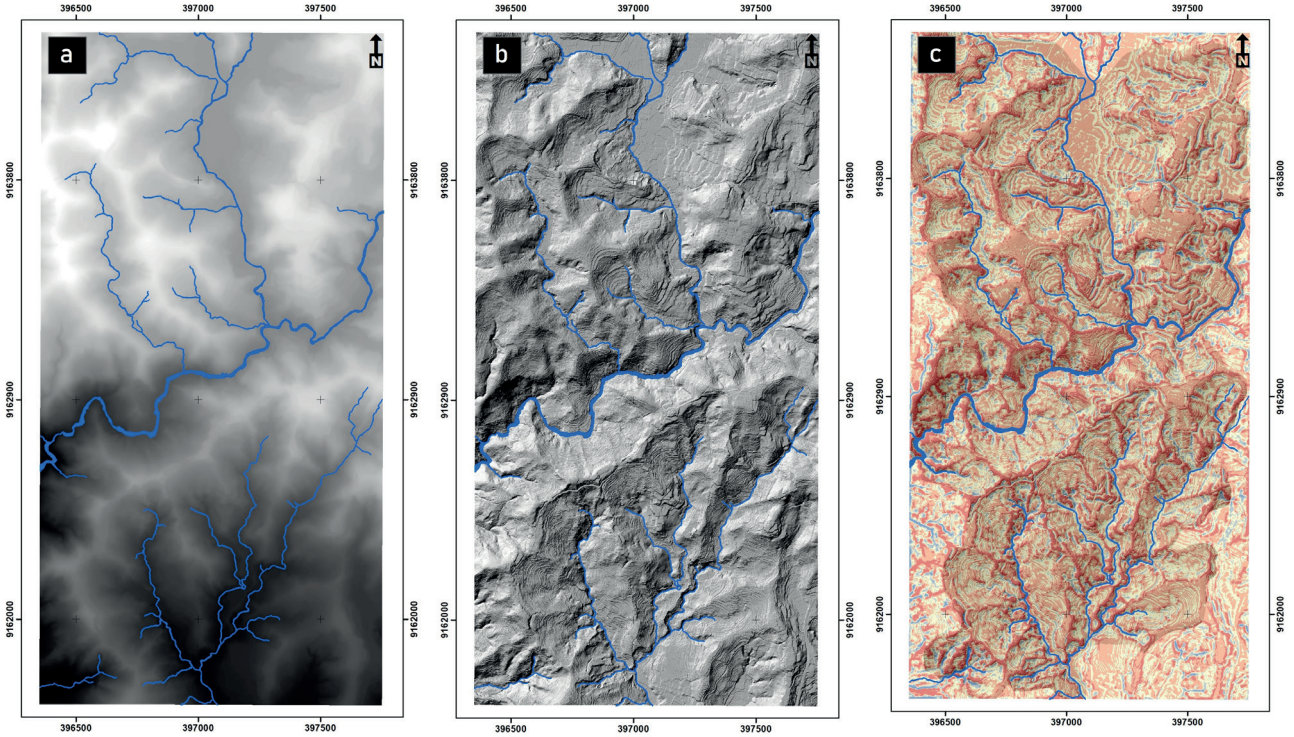

Fig. 3. DTM LiDAR (a) derivatives in the form of Hillshade (b) and Topographic Position Index (TPI) with a 0.5 × 0.5 size of the neighborhood (c)

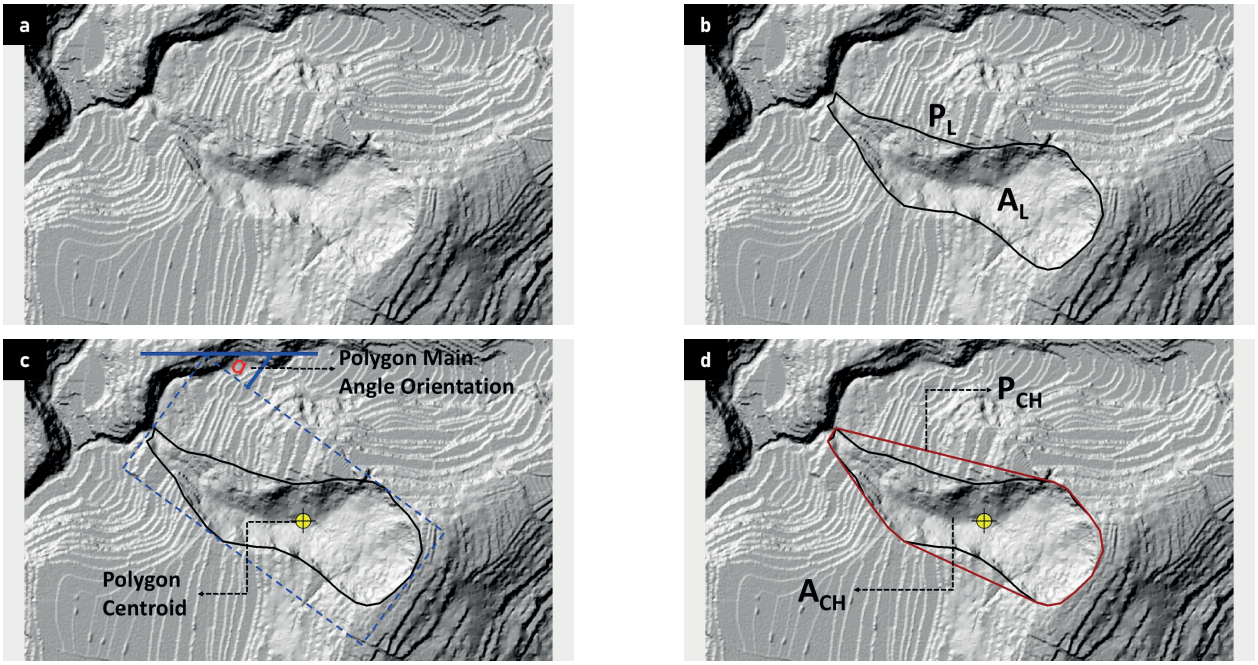

Fig. 4. Derived LiDAR data is used to demarcate the landslide boundary and determine the geometric elements required in the polygon ellipse calculation: (a) landslide feature, (b) area and perimeter of landslide boundary, (c) polygon centroid and its main angle orientation, and (d) area of convex hull and perimeter of convex hull

The landslide boundaries identified in this study were delineated based on surface morphological characteristics. However, many of these areas have since experienced changes in land use and land cover, resulting in the loss of visible landslide features in the field. The landslide delineation resulted in a polygon that was then subjected to a 2D convex hull operation. This operation found the minimum bounding geometry, which was the smallest convex polygon that fit around the input feature. For each resulting polygon obtained from the convex hull analysis, the area (A_{CH}), perimeter (P_{CH}), central coordinates (x, y), and primary angle (α) were also computed.

Mathematical computations were employed to ascertain the length-to-width ratio *(AE)*. The length-to-width ratio and ellipse dimensions were subsequently applied to the convex hull of the polygon (Eq. 1).

$$\Lambda_E = \frac{L_E}{W_E} = \frac{\sqrt[2]{\frac{A \times \Lambda_E}{\pi}}}{\sqrt[2]{\frac{A}{\pi \times \Lambda_E}}} = \frac{4\pi A_E}{P_E^2 - \sqrt{P_E^4 - 16\pi^2 A_E^2}} \quad (1)$$

Λ_E - length-to-width ratio of ellipse
L_E - length of ellipse (m)
W_E - width of ellipse (m)
P_E - perimeter of ellipse (m)

The ellipse was graphically represented using a polygon center point (x, y) endowed with length (*L* scaled *CH*) and width (*W* scaled *CH*) attributes (Eq. 2). The graphical depiction of the polygon ellipse was aligned with the orientation of the landslide. The ellipticity index (e_L) in Eq. 3 was derived from the disparity between the landslide polygon and the ellipse polygon (Lombardo, 2014). An inverse relationship was observed between the size of the area outside the polygon (A_L-$A_{L\cap E}$) and the ellipticity index; specifically, a larger area corresponded to a smaller ellipticity index and vice versa. The ultimate ellipse (Fig. 5) was determined by its area (A_E), perimeter (P_E), length (L_E), width (W_E), semi-major axis (a), and semi-minor axis (b).

$$L_M\left[\left(A_{CH}, P_{CH}\right) \rightarrow A_L\right] = L_M\left[A_{CH}, P_{CH}\right]\sqrt{A_L/A_{CH}}$$
$$W_M\left[\left(A_{CH}, P_{CH}\right) \rightarrow A_L\right] = W_M\left[A_{CH}, P_{CH}\right]\sqrt{A_L/A_{CH}} \quad (2)$$

L_M - length of landslide for elliptic approximation based on convex hull (m)
W_M - width of landslide for elliptic approximation based on convex hull (m)
A_{CH} - area of landslide convex hull (m²)
P_{CH} - perimeter of landslide convex hull (m)
A_L - area of landslide (m²)

$$e_L = 1 - 2\frac{A_L - A_{L\cap E}}{A_L} \quad (3)$$

e_L - ellipticity indexx
A_L - area of landslide (m²)
$A_{L\cap E}$ - area of intersection (∩) between original landslide shape and elliptical approximation (m²)

In the previous method, the arithmetic rotation was used to automatically run polygonal main angle calculations, determining the orientation of a landslide. However, this approach produced a principal angle that did not align with the actual landslide angle. The principal angle in the context of landslides pertains to the spatial arrangement of length and width within a landslide, indicating the direction of the landslide's length from its summit to its base. Slope angles were utilized to assess locations that might become unstable (Donnarumma et al. 2013). It was imperative to rectify the principal angle of the landslide to ascertain the original ellipticity value. This correction was implemented through the application of rotation tools. The numerical representation of the landslide's principal angle indicated the rotational angle value measured from a reference point in the northward direction. The landslide direction is quantified in degrees of rotational angle measured clockwise from the north.

$$\tan\alpha = \frac{H}{L_{CL}}, \quad \alpha = \tan^{-1}\frac{H}{L_{CL}}, \quad L = \sqrt{L_{CL}^2 + H^2} \quad (4)$$

Each landslide is characterized by a principal slope angle formed between the failure surface and the horizontal plane. The landslide polygons, delineated from LiDAR-derived DEM data, provide measurements of the landslide's horizontal length *(Lc)* and vertical height *(H)*, as described in Fig. 6. These parameters are used to calculate the slope angle of the landslide (α) and the landslide's oblique length *(L)*, as defined in Eq. 4.

RESULTS

2D Geometrical Features of Landslide Boundary

Landslide geometry is controlled by the friction angle of the slope's remaining material and its original slope angle. The geometry of a landslide is defined by the ratio of its thickness to its length. We used LiDAR data to observe distinctive features of landslide geometry, enabling the creation of precise landslide boundary areas. Each landslide boundary unit possessed geometric attributes that accurately described its topographic shape,

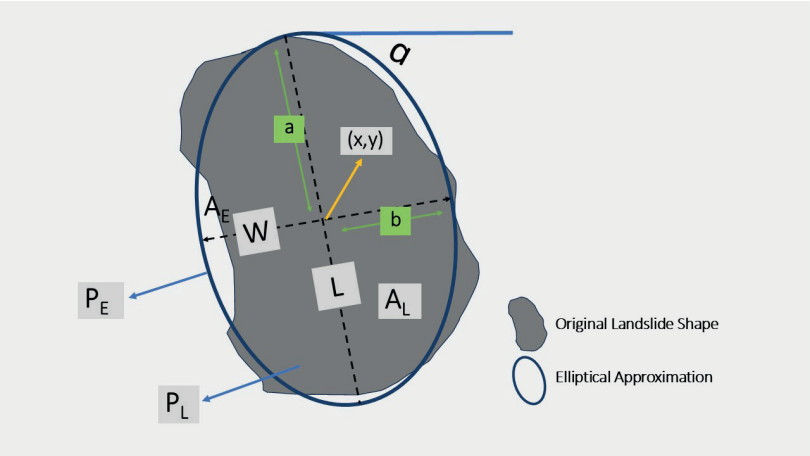

Fig. 5. Plotting Ellipse from LE, WE, centroid (x, y), and orientation (α) (Taylor et al., 2018)

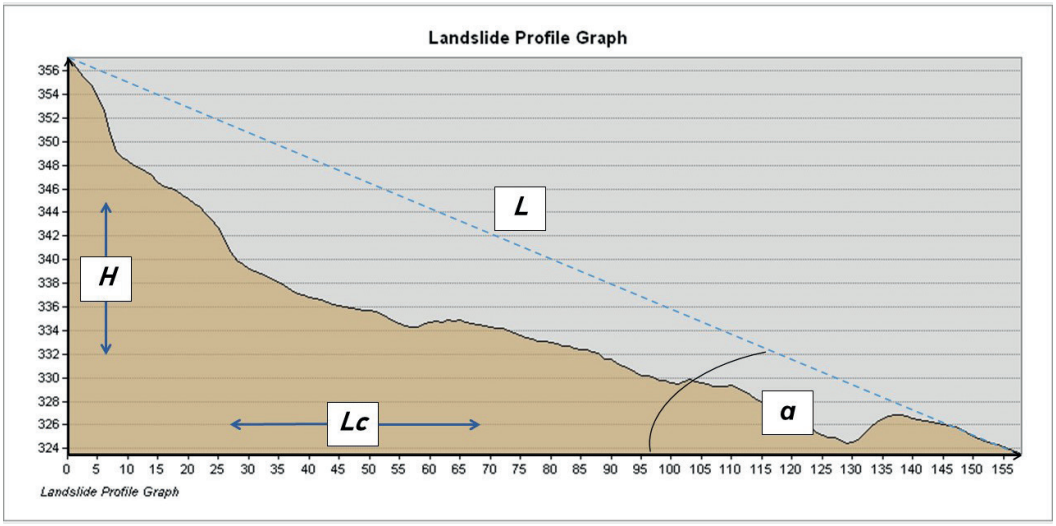

Fig. 6. How to obtain the main slope value from a 2D landslide illustration (example from landslide ID 11)

representing various landslide conditions observed in the field (Fig. 9a). The erosion-deposition process on landslide bodies creates surface shapes with both concave and convex components. These features are illustrated in 2D planes in Fig. 6 and quantified based on area, perimeter, height, width, length, and slope (Table 1).

Landslides affected 72% of the study area, with 259 landslides successfully delineated. The landslide areas ranged from 70 m^2 to 99,627 m^2. We observed a pattern in the configuration of landslide boundary polygons, where small boundary areas typically followed larger ones. Each landslide boundary unit's perimeter showed a strong positive linear relationship (0.82) with its area. The landslide elevation range *(H)*, also referred to as landslide thickness, varied between 1 and 115 m, showing a weak positive linear relationship (0.34) with area. The average landslide length at the centerline *(L_{CL})* was shorter than the total length *(L)* because L included the landslide runout distance. Landslide thickness was proportional to length, with their ratio determining the overall landslide geometry. Landslide boundary unit widths ranged from 6.18 to 503.51 m. The landslide slope angle (α) varied with the landslide area, with steeper angles typically occurring in smaller landslides.

Landslide Ellipticity

The ellipticity index in the study area ranged from -0.74 to 0.96 (Fig. 7). By using the geometrical interval classification technique, the ellipticity index *(e_L)* was categorized into two classes: -0.74 to 0.63 (non-ellipse), and 0.63 to 0.96 (ellipse). The classification technique employed in this study aimed to represent continuous data visually, and the advantage of the geometric interval's classification is its ability to effectively handle data that do not follow a normal distribution. The study site exhibited a prevalence of high eL values, with 137 ellipse polygons and 122 non-ellipse polygons. We observed that the average landslide area decreased as the eL values increased, indicating a transition towards a more elliptical shape. This pattern indicates that smaller landslides tend to adopt more defined elliptical forms, while larger ones display more variability in

Table 1. Statistic parameters for 2D landslide geometry

Statistic Parameters	A_L	P_L	H	W	L_{CL}	L	α
Mean	8839.88	392.72	26.12	74.45	94.38	98.64	18.47
Standard Error	1010.21	26.31	1.08	4.39	5.56	5.61	0.47
Median	2680.32	227.61	20.00	47.66	62.00	65.07	17.65
Mode	#N/A	#N/A	14.00	35.02	42.00	55.71	16.70
Standard Deviation	16257.81	423.48	17.31	70.58	89.45	90.33	7.52
Sample Variance	264316351.59	179334.71	299.72	4981.75	8000.48	8158.99	56.61
Kurtosis	13.71	6.60	2.15	8.65	6.45	6.07	0.35
Skewness	3.50	2.42	1.22	2.46	2.35	2.28	0.50
Range	99556.90	2600.04	114.00	497.33	530.00	533.12	41.09
Minimum	69.80	36.83	1.00	6.18	10.00	11.40	2.64
Maximum	99626.70	2636.87	115.00	503.51	540.00	544.52	43.73
Sum	2289530.00	101713.62	6764.00	19283.43	24444.00	25547.93	4784.30
Count	259	259	259	259	259	259	259

A_L = landslide area (m^2), P_L = landslide perimeter (m), H = landslide elevation range (m), W = landslide width (m), L_{CL} = landslide length centerline (m), L = landslide total length (m), α = landslide slope angle (°)

shape. Such distinctions carry important implications for landslide risk assessment, as the morphology of a landslide may reflect its activity status. Landslides with well-preserved elliptical shapes, which have not experienced significant morphological modification, may indicate a higher potential for reactivation. In contrast, landslides whose shapes have evolved through multiple modification processes are likely associated with greater slope stability. Understanding this relationship between shape, size, and stability can support more accurate predictive modeling and guide targeted land use planning and mitigation efforts in susceptible regions.

Based on the results of aerial imagery captured in 2024, followed by ground-truthing through a field survey, 48 landslides are identified as falling within the active state. These recently occurring landslides are categorized as both ellipse and non-ellipse. Active landslides are particularly observed on depositional slopes, which are closely associated with loose soil material and its high-water retention capacity. Depositional slopes often consist of unconsolidated sediments, which are more prone to failure compared to lithified material. The loose nature of these sediments makes them susceptible to landslides, especially when combined with other triggering factors such as rivers. As a result, the dynamic flow of river water continuously influences newly formed landslides, causing modifications to the contours of the landslide boundary so that the shape can be an ellipse or non-ellipse.

Landslide direction pertains to the specific orientation or azimuth in which a slope undergoes a landslide event (Massey et al. 2013). In the investigated area, landslides predominantly manifest in the south, southeast and southwest directions (Fig. 8). How landslides move is closely connected to how the regional geological structures are shaped in the study area through local lineaments. The river flow pattern, which consists of intermittent rivers that typically flow from north to south before merging into perennial rivers that stream from northeast to southwest, illustrates the control of the geological structure (Patanduk 2020).

Landslide Ellipticity	Number of Landslide
-0.74 – 0.63 (non-ellipse)	122 (47%)
0.63 – 0.96 (ellipse)	137 (53%)

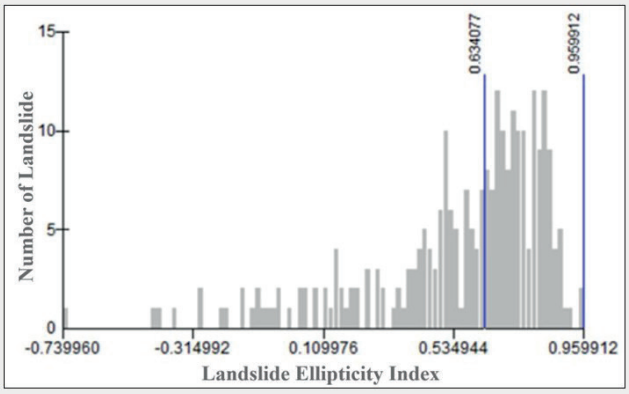

Fig. 7. Division of ellipticity index classes using the geometrical interval classification technique

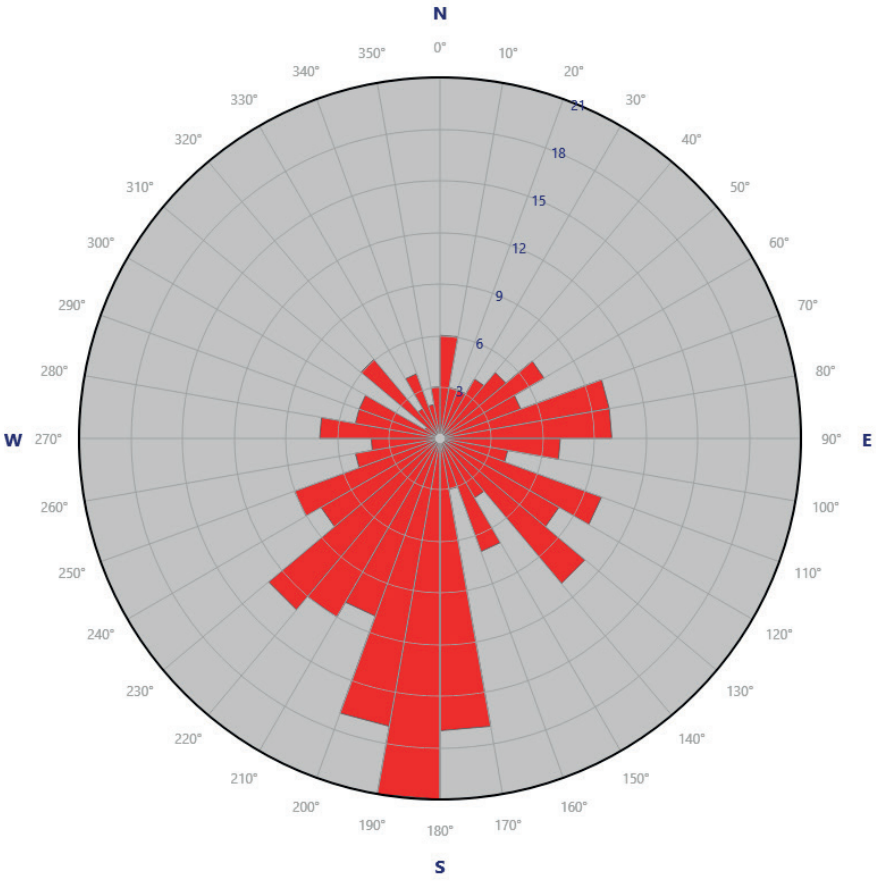

Fig. 8. The orientation of 259 landslide units within the study area is presented in a rose diagram, revealing a dominant directional trend toward the southeast, south, and southwest

Land Use and Land Cover

Land use types were interpreted from aerial photography and were classified into nine types (Fig. 9c). As presented in Table 2, the dominant land use was mixed gardens (73%). Following closely was the allocation of 18% to rice fields, houses 3%, dry field agriculture 3%, with the remaining 3% encompassing bare land, roads, and water bodies such as rivers. Rice fields exhibited a widespread distribution across valleys and inclined terrain, while dry field agriculture was dispersed proximately to these paddy fields. Houses tended to show a distribution pattern that was dominated by occupying high positions along the hillsides. The presence of bare land exhibited a random arrangement interspersed among mixed gardens and was notably associated with areas susceptible to new landslide occurrences. Intermittent rivers indicated a directional alignment from north to south, while the perennial river followed a northeast-southwest line. In the irrigated rice field land use unit, there are irrigation canals located on the slopes, interconnected with adjacent groups of irrigated rice fields. Small-sized ponds were also found that were intended for cultivating freshwater fish, most of which were located near irrigated rice fields.

DISCUSSION

Relation between Landslide Ellipticity and 2D Geometrical Features

Large dormant landslides are often accompanied by smaller, active landslides in the present day. There is a tendency for high ellipticity to occur in small landslides. This observation supports the theory that current geomorphological processes continue but with diminishing intensity over time (Guzzetti et al. 2012). The increasing steepness of slope angles following successive landslides demonstrates the dynamic equilibrium effect, where land surfaces tend toward flatness over time (Roering and Hales 2022). However, recent surface processes typically produce significantly steeper slope angles. The descriptive presentation in Fig. 10 shows that elliptical

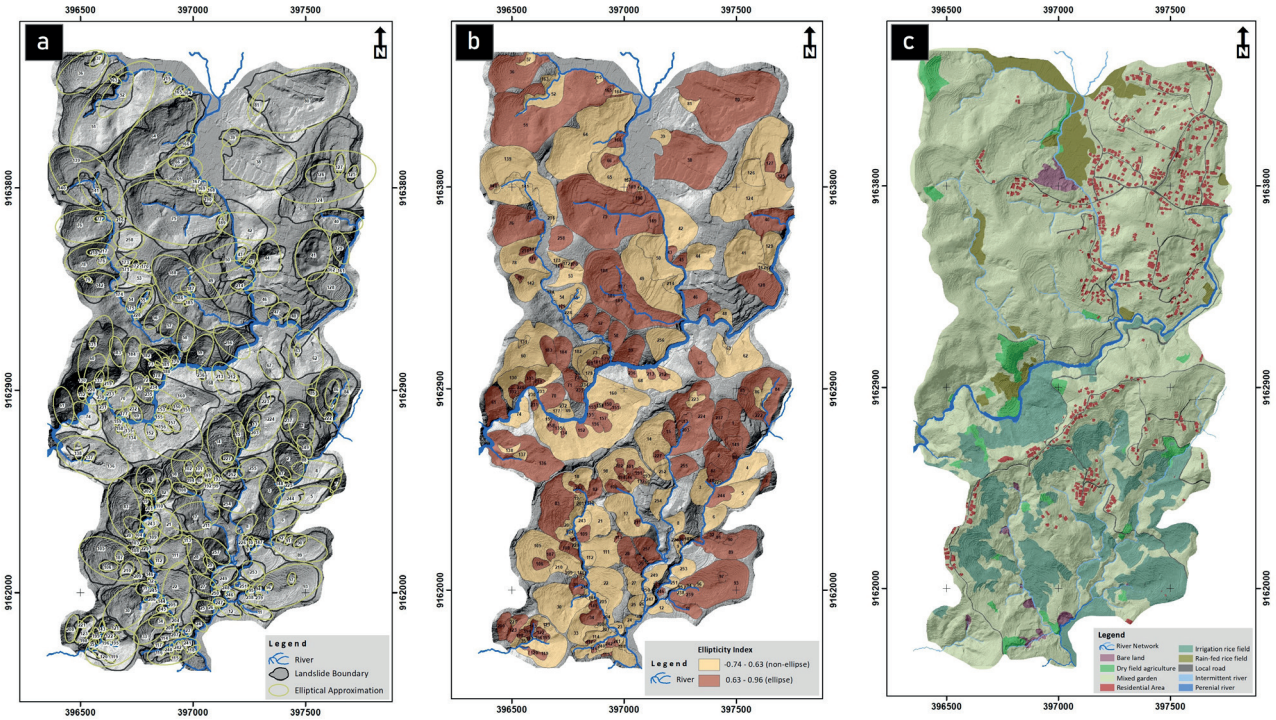

Fig. 9. (a) Mapped landslide boundary and its elliptical approximation, (b) Landslide ellipticity index, (c) Land use land cover in the key research area

Table 2. Land use land cover in the study area

No	Land Use Land Cover	Area within the study area (m^2)	%	Area within landslide boundary (m^2)	%
1	Bare land	25,750.73	0.81	24,706.74	1.08
2	Dry field agriculture	86,996.34	2.75	65,441.32	2.86
3	Houses	107,974.16	3.41	61,359.48	2.68
4	Intermittent river	15,158.46	0.48	4,972.18	0.22
5	Irrigated rice field	434,197.44	13.71	351,835.22	15.37
6	Local road	39,270.29	1.24	19,914.60	0.87
7	Mixed garden	2,317,471.15	73.18	1,729,790.30	75.55
8	Perennial river	22,314.18	0.70	2,862.75	0.13
9	Rain-fed rice field	117,504.15	3.71	28,647.43	1.25
Total		3,166,636.90	100	2,289,530.02	100

landslides are small and have relatively minor geometric parameters, particularly in the area value, perimeter, width, and elevation range. The Ellipse category is found with an average landslide size of 8175 m^2, an average perimeter of 338 m, an average width of 60 m, and an elevation range of 31 m. Meanwhile, the non-ellipse class occurred in landslides with a size of 9587 m^2, an average perimeter of 455 m, an average width of 91 m, and an elevation range of 30 m. Meanwhile, the *L* size in the ellipse category is 102 m, and in the non-ellipse category, it is 98 m. The average size of L_{CL} in the ellipse category is 117 m, and in the non-ellipse category, it is 108 m.

The geometry of the landslide, which is reflected in the ellipticity index at the research location, has varying slope angles. Landslides with steep slopes can occur in ellipse or non-ellipse conditions, and vice versa, landslides with small slopes can also occur in both. The average landslide angle at the research location, whether elliptical or non-elliptical, is 18.4 degrees. Slope size is one of the most important factors influencing slope instability as a cause of landslides. The magnitude of the landslide slope angle is inversely proportional to the landslide volume, indicating that there is a difference in the control of the slope angle on the size of the landslide for a certain material strength (Fan 2010; Li and Kong 2010; Wu et al. 2024). This condition explains how the landslide slope is affected by local situations such as slope height, soil material, landslide slip surface, and its spatial arrangement.

Relations between Landslide Ellipticity and Land Use Land Cover

Land use and land cover are some of the factors that determine the occurrence of landslides (Bartelletti et al. 2017; Cevasco et al. 2014), and the land use changes caused by human activities have a significant impact on the onset of landslide events (Meneses et al. 2019). The resulting landslide's surface shape varies depending on its LULC. This study's analysis considers nine classes of LULC at the research location. The assessment of the level of ellipticity of landslide scars in LULC units is also deepened by the trend of geometrical feature conditions. The condition of the tendency for landslides to be long-short, large-small, wide-narrow and the size of the slope angle can be seen in Fig. 12.

The boxplot in Fig. 11 illustrates the distribution of ellipticity index values for each LULC. We chose the boxplot visualization to precisely compare the distribution of each set of ellipticity values, particularly within the LULC group, and understand their range. Perennial rivers have the highest median value, 0.61, while house units have the lowest, 0.455. The spread of the distribution describes the difference between quartile 3 (upper whisker) and quartile 1 (lower whisker). The widest distribution of eL values is on local roads with a value of 0.6, followed by houses with a value of 0.585 and mixed gardens with a value of 0.545. The perennial river has the smallest distribution; the result can be seen from the thin bar diagram.

From minimum to maximum, the range (largest minus smallest) shows the width of all data. The range can be seen from the length of the lower and upper fences. The largest range occurs in mixed garden units with the lowest e_L data, namely -0.74, and the highest e_L data is 0.95. The smallest range is owned by rain-fed rice fields with the lowest e_L data, namely -0.11, and the highest e_L data, 0.96. The shape of the e_L distribution based on land use units illustrates whether the e_L value is normally distributed or not. A normal distribution can be seen if the middle 50% of the data is evenly divided, with 25% of the data between quartile 1 and quartile 2 equal to 25% of the data between quartile 2 and quartile 3. We found no normal distribution of 9-unit land use based on the eL value. The shape of the distribution of 9-unit land use is skewed left, which shows the dominance of the data

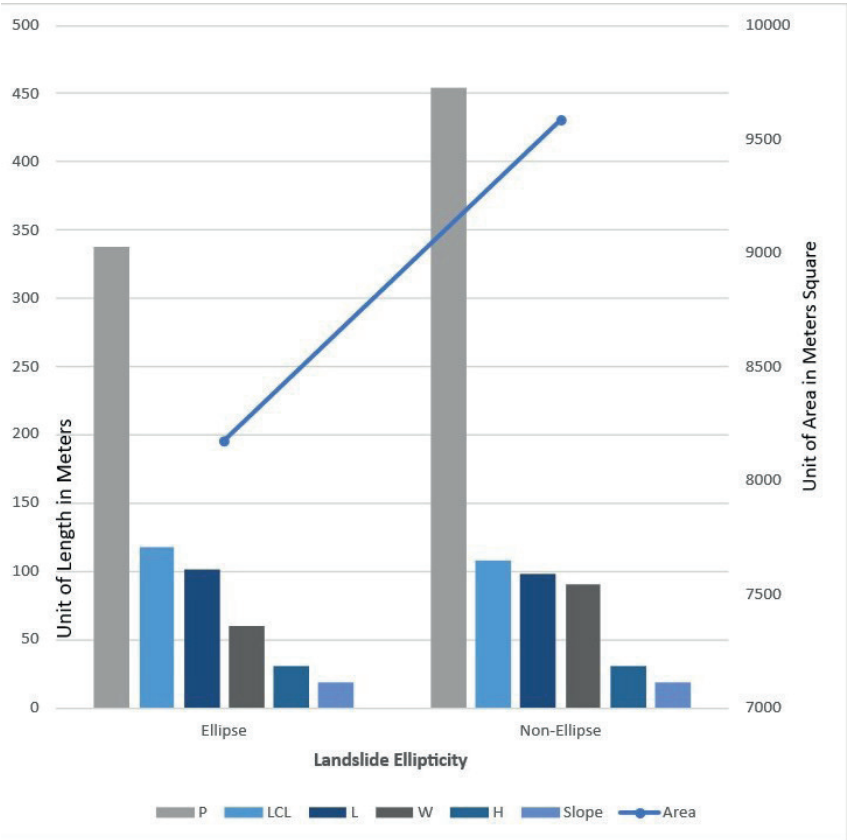

Fig. 10. The relationship between landslide ellipticity and the average value of 2D geometrical features (*P*: Landslide perimeter in meters, L_{CL}: Landslide center length in meters, *L*: Landslide total length in meters, *W*: Landslide width in meters, *H*: Landslide height in meters, Slope was in degrees, and Area was in meter square)

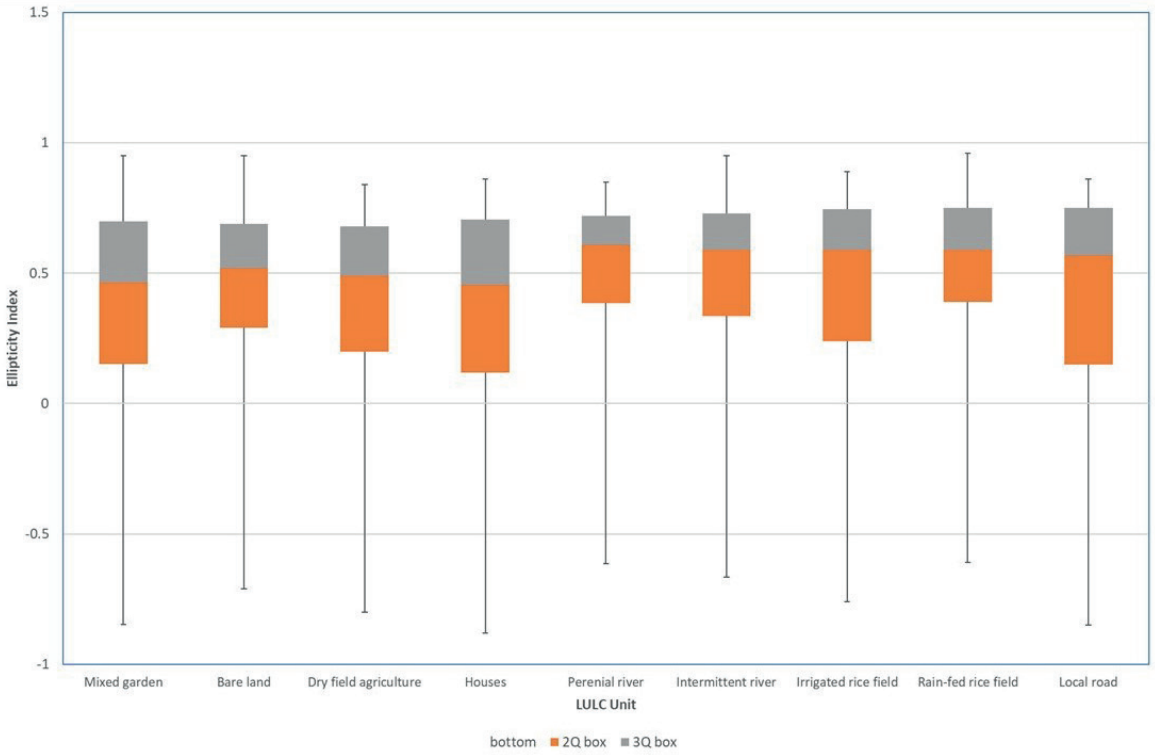

Fig. 11. Boxplot of the landslide ellipticity index distribution for each LULC unit

distribution below the median value (quartile 3). From Fig. 8, it can be concluded that LULC units with high ellipticity include bare land, mixed gardens, rain-fed rice fields, and intermittent rivers, while LULC with low ellipticity occurs in local roads, houses, irrigated rice fields, and mixed gardens.

As shown in Fig. 11, sequentially, the dominance of the highest e_L is bare land, mixed gardens, rain-fed rice fields, and intermittent rivers. High-ellipticity landslides are active landslides that have just occurred, so they still have elliptical boundaries. The recent landslide that occurred in less than 1.5 years means that the land cover above the landslide is currently bare land. Geometrically, landslides on bare land are small, short, and narrow, and they have steep slopes (Fig.12). These landslides are located along intermittent rivers on a spatial scale. Intermittent rivers flow only during certain times of the year when there is sufficient rainfall.

The mixed garden at the study location is dominated by woody plants, which vary in terms of tree height and tree types with low-to-high density levels. High e_L was found in landslides in low-density mixed-garden areas. Landslides found in mixed garden units are characterized by small, short, narrow geometry with slope sizes tending to be large (Fig. 12). This situation strengthens the evidence that many new and active landslides have been found in landscapes with mixed garden cover. The presence of various plant species and their alterations in the mixed garden area are expected to impact the soil's shear strength, leading to slope instability. In certain instances, these rapid changes can potentially initiate landslides (Davies 2015). Detailed observation of aerial photos of the active landslide polygons reveals a land cover pattern in the form of mixed gardens with sparse density and coconut trees at the top of the slope.

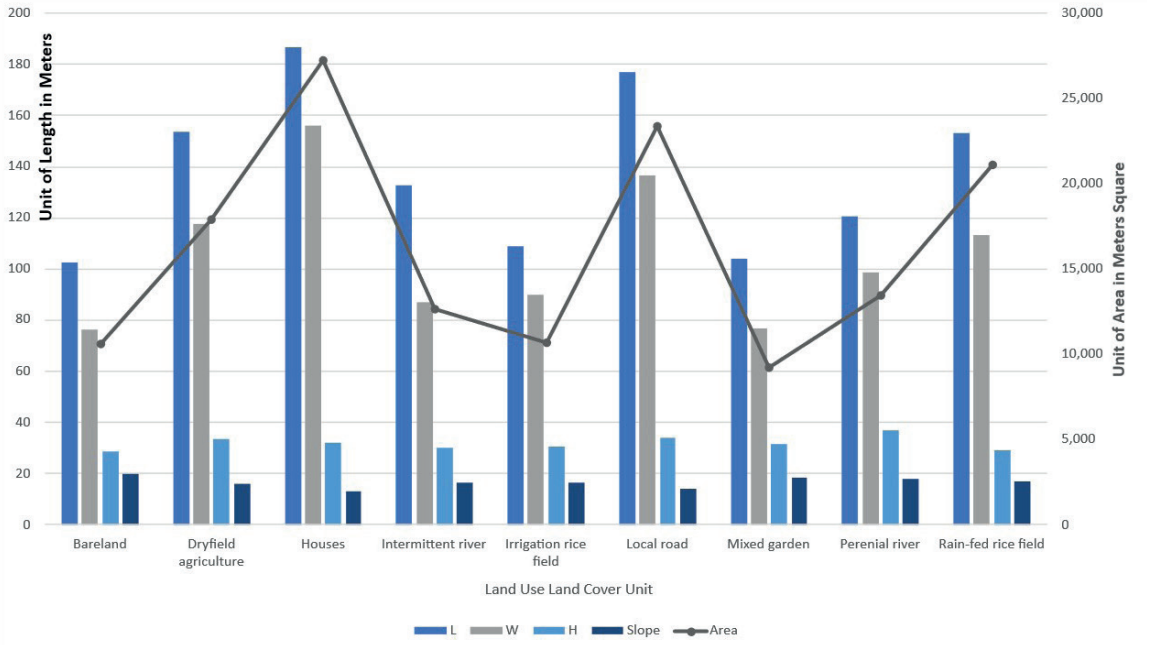

Fig. 12. Trends in 2D geometrical landslide features on LULC units, considering landslide total length in meters (*L*), landslide width in meters (*W*), landslide height in meters (*H*), landslide slope in degrees, and landslide area in square meters

The rain-fed rice fields scattered between the foot slopes of the quarter-tertiary volcanic slopes are only planted once a year on average. Rain-fed rice fields will only be cultivated intensively when the rainy season arrives. Intercrops in the growing season after rice are usually secondary crops, such as corn and horticulture. The landslides found on this land use have a larger geometric character, are a little longer, and have a narrow geometry with slope sizes tending to be large.

Specifically, the active landslides occur on depositional slopes intimately connected to water and river dynamics. The phenomenon of riverbank undercutting arises from the rapid flow of water at bends or specific segments of the river (Figs. 13a, c, e). Elevated water pressure induces erosion along slopes and riverbanks. The progressive undercutting at the base generates instability in the overlying slope, leading to subsequent collapse. As a result, the dynamic flow of river water continuously influences newly formed landslides, causing modifications to the contours of the landslide boundary, whether ellipse or non-ellipse. From the Fig. 11 graph, the landslides along the intermittent river are wide, so some of the final landslides along the river channel have a non-ellipse shape.

The distribution of low ellipticity values is owned by local roads, houses, irrigated rice fields, and mixed garden units. Landslide boundary units with irregular or non-ellipse shapes are greatly influenced by the intensity of land management (Kimura 2024; Segoni et al. 2024). The predominance of low ellipticity occurs in areas of former landslides crossed by local roads, caused by cut and fill slopes during the construction process (Figs. 13f, g, h). Slope modification has a high influence on changing the features of past landslides into non-elliptical ones (Sartohadi et al. 2024). If viewed on a site-specific basis, slope modification can increase slope instability (Jaboyedoff et al. 2016). The landslide geometry in the local road unit is larger, longer, and wider with a smaller slope (Fig. 11). Road construction and maintenance have direct or indirect impacts on slopes through slope cuts or changes in surface water runoff (Vuillez et al. 2018). The accumulation of water runoff that leads to landslide slip areas has the potential to trigger landslides (Ran et al. 2018). Additional effects on roads encompass the establishment of logging pathways which typically adhere to distinct standards in contrast to the official road regulations (Jaafari et al. 2015), which generally follow different regulations compared to official road regulations. With a minimum standard size and quality, the existence of roads in the village is also the main route used for transporting building materials and harvesting products with quite a large tonnage. Vehicle traffic with heavy loads has an impact on road stability which can trigger landslide reactivation.

Most of the houses are in flat areas, either at the top of slopes or valley plains. The current flat condition is likely to occur due to two things, occurring naturally through the erosion-deposition process during land sliding or the process of human civilization when constructing the settlement through slope modification. The 2D feature values in landslides in houses have large sizes, widths, and slopes tend to be smaller (Fig. 12). Houses and local roads are positioned at the top of slope areas, which could be the cause of landslides. Rainwater falls on residential roofs and local roads at the start of the rainy season, significantly contributing to surface flow, which then triggers the process of wetting the landslide slip surface. This concentrated surface flow acts as a source of energy that causes gully erosion and landslides (Shen et al. 2022).

Irrigated rice fields are agricultural land uses with the highest management intensity. An irrigation network follows the distribution of irrigated rice fields in the study location, which also features several fish ponds. The irrigated rice fields at the study location have terraces developed in a regular pattern following the slope pattern. A flat terrace surface will hinder surface flow and transport of soil material, but on the other hand, it will allow greater water infiltration. This event has an important role in wetting the landslide slip surface, especially the subsurface soil material, which is more impermeable. The results of a literature review (Garcia-Chevesich et al. 2021; Segoni et al. 2024) show that landslides caused by irrigation are an increasing risk in regions where there are agriculture and certain climatic and geological conditions. The characteristics of former landslides at this stage include slopes of less than eight degrees and intensive management for agriculture with more regular terracing applications. Between the terraces, there are small areas containing a group of vegetation as mixed gardens. Woody vegetation is also found extending at the foot of the slopes along the river. Land cover, especially vegetation conditions, tends to be uniform throughout the area.

Landslides with low ellipticity also occur in mixed gardens. A non-ellipse mixed garden has a different geometric character from an ellipse mixed garden, where the landslide size is larger and the slope angle tends to be smaller. The diversity of vegetation in a low ellipticity mixed garden consists of multilayer crops. Multilayer vegetation tends to stabilize slopes by anchoring soil and reducing surface runoff (Fattet et al. 2011). However, mixed gardens with low ellipticity are located close to house complexes and road networks so the intensity of maintenance, management, and harvesting of garden products is higher. High-pressure management in mixed gardens has a big role in changing the shape of landslide scars to become irregular.

The results of landslide boundary shape identification and each of its geometric characteristics serve as a significant standard for land management methods. The

Fig. 13. Active landslides were found during the field survey. (a – e) active landslides in mixed gardens adjacent to rice fields and river, (f – h) active landslides over residential areas

landslide boundary configuration is characterized by an elliptical shape, indicating recent landslide events, and post-landslide land use. The occurrence of new landslides raises concerns about the stability of the land, which is yet uncertain. Therefore, it is crucial to consider more controlled land use in areas that have recently experienced landslides. Utilizing unstable terrain without any limitations carries a substantial danger of incurring losses. After a landslide occurs, it is wise to adopt agroforestry techniques for dry field agriculture in the early stages (Garrity 2012) which provides the possibility of increasing the shear strength of the soil. Feasible cultivation of crops for dryland agriculture can be achieved by considering the stability of previous landslide-prone slopes and effectively addressing the risks of erosion and reactivation of landslides (Purwaningsih et al. 2020).

The landslide boundary is shaped in an irregular or non-elliptical form, representing an inactive landslide, with more stable slopes. Land located in places with low ellipticity can be effectively utilized for a diverse range of uses. The landslide boundary located adjacent to the ellipse in inactive landslides exhibits a range of slope conditions, ranging from flat to extremely steep. An important thing that must be considered in land use management is how to minimize the wetting of landslide slip areas when it rains, which can produce runoff that ultimately triggers landslides. Land use planning prioritizes the assessment of local landslide slopes, particularly focusing on the crown, scarp, sides, landslide body, and landslide foot. Every component of the landslide possesses a distinct ecological role, necessitating appropriate adjustments in land utilization. The combination of the preexisting landslide boundary shape and its land use serves as the primary input for generating suggestions for the detailed land use planning management. Implementing local-level planning measures is crucial for mitigating the ecological and economic damages caused by landslides.

CONCLUSIONS

Land use and land cover patterns play a fundamental role in determining both the occurrence of landslides and the morphology of resulting landslide surfaces. Our research reveals that changes in surface geomorphological features, particularly landslide boundaries, are intimately connected to temporal variations in land use and cover patterns. Analysis of two-dimensional landslide boundaries in the study area revealed distinct elliptical and non-elliptical configurations. The ellipticity index in the study area ranged from -0.74 to 0.96.

Small, active landslides, often elliptical in shape, occur alongside larger dormant ones, reflecting ongoing but diminishing geomorphic processes that result in steeper slopes and distinct geometric characteristics, with elliptical slides showing smaller area, perimeter, and width than non-elliptical types. Landslide geometry, as indicated by ellipticity and an average slope angle of 18.4°, is not solely dependent on shape but is influenced by local factors such as slope height, soil material, and slip surface, with steeper slopes generally associated with smaller landslide volumes, highlighting the inverse relationship between slope angle and landslide size under consistent material strength.

Landslide direction in the study area predominantly follows south to southwest orientations, reflecting the influence of regional geological structures and local lineaments, as further evidenced by river flow patterns shaped by structural controls that channel water from north to south and then southwest.

Elliptical landslide boundaries (-0.74 to 0.63) predominantly occur in areas of bare land, mixed gardens, rain-fed rice fields, and intermittent rivers. These elliptical patterns are typically associated with lands characterized by minimal management intensity and unstable slope conditions, underscoring the need for careful land management strategies that prioritize slope stability. In contrast, non-elliptical landslide boundaries (0.63 to 0.96) are primarily observed in areas with significant infrastructure development, including roads, housing developments, irrigated rice fields with canal systems, and managed mixed gardens. These non-elliptical patterns generally correspond to areas with intensive land management and relatively stable slope conditions. However, even in these more stable areas, careful attention must be paid to factors that could trigger slope failure, particularly the saturation of potential slip surfaces that might reactivate dormant landslides.

REFERENCES

Bartelletti C., Giannecchini R., D'Amato Avanzi G., Galanti Y., and Mazzali A. (2017). The influence of geological-morphological and land use settings on shallow landslides in the Pogliaschina T. Basin (northern apennines, Italy). Journal of Maps, 13(2). DOI: 10.1080/17445647.2017.1279082.

Bruschi V. M., Bonachea J., Remondo J., Gómez-Arozamena J., Rivas V., Méndez G., Naredo, J. M., and Cendrero A. (2013). Analysis of geomorphic systems' response to natural and human drivers in northern Spain: Implications for global geomorphic change. Geomorphology, 196. DOI: 10.1016/j.geomorph.2012.03.017.

Cevasco A., Pepe G., and Brandolini P. (2014). The influences of geological and land use settings on shallow landslides triggered by an intense rainfall event in a coastal terraced environment. Bulletin of Engineering Geology and the Environment, 73(3). DOI: 10.1007/s10064-013-0544-x.

Chen A., Darbon J. Ô., and Morel, J. M. (2014). Landscape evolution models: A review of their fundamental equations. Geomorphology, 219, 68–86. DOI: 10.1016/J.GEOMORPH.2014.04.037.

Chen L., Guo Z., Yin K., Pikha Shrestha D., and Jin S. (2019). The influence of land use and land cover change on landslide susceptibility: A case study in Zhushan Town, Xuan'en County (Hubei, China). Natural Hazards and Earth System Sciences, 19(10). DOI: 10.5194/nhess-19-2207-2019.

Davies T. (2015). Landslide Hazards, Risks, and Disasters: Introduction. In Landslide Hazards, Risks, and Disasters. DOI: 10.1016/B978-0-12-396452-6.00001-X.

Dhingra R. D., Barnes J. W., Hedman M. M., and Radebaugh J. (2019). Using Elliptical Fourier Descriptor Analysis (EFDA) to Quantify Titan Lake Morphology. The Astronomical Journal, 158(6). DOI: 10.3847/1538-3881/ab4907.

Donnarumma A., Revellino P., Grelle G., and Guadagno F. M. (2013). Slope angle as indicator parameter of landslide susceptibility in a geologically complex area. Landslide Science and Practice: Landslide Inventory and Susceptibility and Hazard Zoning, 1. DOI: 10.1007/978-3-642-31325-7_56.

Fan X. Y. (2010). Comparative study of movement behaviors of seismic and non-seismic induced landslides. Yantu Lixue/Rock and Soil Mechanics, 31(SUPPL. 2).

Fang Y., Xu Q., Chen J., Li J., and Zhang T. (2024). Investigating landslide-induced tsunamis using a low-dissipation Riemann weakly compressible smoothed particle hydrodynamics model. Elsevier. DOI: 10.1016/J.OCEANENG.2024.118512.

Fattet M., Fu Y., Ghestem M., Ma W., Foulonneau M., Nespoulous J., Le Bissonnais Y., and Stokes A. (2011). Effects of vegetation type on soil resistance to erosion: Relationship between aggregate stability and shear strength. Catena, 87(1). DOI: 10.1016/j.catena.2011.05.006.

Fell R., Corominas J., Bonnard C., Cascini L., Leroi, E., and Savage W. Z. (2008). Guidelines for landslide susceptibility, hazard, and risk zoning for land use planning. Engineering Geology, 102(3–4). DOI: 10.1016/j.enggeo.2008.03.022.

Garcia-Chevesich P., Wei X., Ticona J., Martínez G., Zea J., García V., Alejo F., Zhang Y., Flamme H., Graber A., Santi P., McCray J., Gonzáles E., and Krahenbuhl R. (2021). The impact of agricultural irrigation on landslide triggering: A review from chinese, english, and Spanish literature. In Water (Switzerland) (Vol. 13, Number 1). DOI: 10.3390/w13010010.

Garrity D. (2012). Agroforestry and the Future of Global Land Use. DOI: 10.1007/978-94-007-4676-3_6.

Guo W. Z., Chen Z. X., Wang W. L., Gao W. W., Guo M. M., Kang H. L., Li P. F., Wang W. X., and Zhao M. (2020). Telling a different story: The promote role of vegetation in the initiation of shallow landslides during rainfall on the Chinese Loess Plateau. Geomorphology, DOI: 10.1016/j.geomorph.2019.106879.

Hooke J. M. (2020). Changing landscapes: Five decades of applied geomorphology. Geomorphology, 366. DOI: 10.1016/j.geomorph.2019.06.007.

Jaafari A., Najafi A., Rezaeian J., Sattarian A., and Ghajar I. (2015). Planning road networks in landslide-prone areas: A case study from the northern forests of Iran. Land Use Policy, 47. DOI: 10.1016/j.landusepol.2015.04.010.

Jaboyedoff M., Michoud C., Derron M. H., Voumard J., Leibundgut G., Sudmeier-Rieux K., Michoud C., Nadim F., and Leroi, E. (2016). Human-Induced Landslides: Toward the analysis of anthropogenic changes of the slope environment. Landslides and Engineered Slopes. Experience, Theory and Practice, 1. DOI: 10.1201/b21520-20.

Jin Z., Hilton R. G., West A. J., Li G. K., Zhang F., Wang J., Li G., Fan X., and Hsieh M. L. (2021). The role of earthquake-induced landslides in erosion and weathering from active mountain ranges: Progress and perspectives. In Science China Earth Sciences (Vol. 64, Number 12). DOI: 10.1007/s11430-021-9832-3.

Kimura T. (2024). Effects of Land Cover Changes and Rainfall Variation on the Landslide Size–Frequency Distribution in a Mountainous Region of Western Japan. Geosciences (Switzerland), 14(3). DOI: 10.3390/geosciences14030059.

Li H., He Y., Xu Q., Deng J., Li W., and Wei Y. (2022). Detection and segmentation of loess landslides via satellite images: a two-phase framework. Landslides, 19(3). DOI: 10.1007/s10346-021-01789-0.

Li X. Z., and Kong J. M. (2010). Runout distance estimation of landslides triggered by "5·12" Wenchuan earthquake. Sichuan Daxue Xuebao (Gongcheng Kexue Ban)/Journal of Sichuan University (Engineering Science Edition), 42(5).

Liu X., Peng Y., Lu Z., Li W., Yu J., Ge D., and Xiang W. (2023). Feature-Fusion Segmentation Network for Landslide Detection Using High-Resolution Remote Sensing Images and Digital Elevation Model Data. IEEE Transactions on Geoscience and Remote Sensing, 61. DOI: 10.1109/TGRS.2022.3233637.

Lombardo U. (2014). Quantitative morphometric analysis of lakes using GIS: Rectangularity R, ellipticity E, orientation O, and the rectangularity vs. ellipticity index, REi. Cartography and Geographic Information Science, 41(4). DOI: 10.1080/15230406.2014.919540.

Martel S. J. (2004). Mechanics of landslide initiation as a shear fracture phenomenon. Marine Geology, 203(3–4). DOI: 10.1016/S0025-3227(03)00313-X.

Massey C. I., Petley D. N., and McSaveney M. J. (2013). Patterns of movement in reactivated landslides. Engineering Geology, 159. DOI: 10.1016/j.enggeo.2013.03.011.

Meneses B. M., Pereira S., and Reis E. (2019). Effects of different land use and land cover data on the landslide susceptibility zonation of road networks. Natural Hazards and Earth System Sciences, 19(3). DOI: 10.5194/nhess-19-471-2019.

Noviyanto A., Sartohadi J., and Purwanto B. H. (2020). The distribution of soil morphological characteristics for landslide-impacted Sumbing Volcano, Central Java - Indonesia. Geoenvironmental Disasters, 7(1). DOI: 10.1186/S40677-020-00158-8.

Ogita S., Sagara W., and Higaki D. (2017). Shapes and Mechanisms of Large-Scale Landslides in Japan: Forecasting Analysis from an Inventory (WCoE 2014–2017). In Advancing Culture of Living with Landslides. DOI: 10.1007/978-3-319-59469-9_26.

Otgonbayar M., Tsedevdorj S.-O., Bumtsend B., Enkhjargal O., and Tovuudorj R. (2023). Spatial Relationships between Topographic Variables and Their Interactions with Natural and Climatic Zonalization in Mongolia. European Modern Studies Journal, 7(5). DOI: 10.59573/emsj.7(5).2023.10.

Patanduk A. (2020). Integrasi Metode Foto udara, GNSS dan Seismik Refraksi Untuk Identifikasi Karakteristik Retakan Permukaan Pada Area Longsor Kalisari, Sub DAS Bompon, Magelang, Jawa Tengah. Tesis. Universitas Gadjah Mada. https://etd.repository.ugm.ac.id/penelitian/detail/187118.

Pirajno F. (2009). Hydrothermal processes and mineral systems. Springer.

Pratiwi E. S., Sartohadi J., and Wahyudi. (2019). Geoelectrical Prediction for Sliding Plane Layers of Rotational Landslide at the Volcanic Transitional Landscapes in Indonesia. IOP Conference Series: Earth and Environmental Science, 286(1). DOI: 10.1088/1755-1315/286/1/012028.

Pudasaini S. P., and Krautblatter M. (2021). The mechanics of landslide mobility with erosion. Nature Communications, 12(1). DOI: 10.1038/s41467-021-26959-5.

Pulungan N. A., and Sartohadi J. (2018). New Approach to Soil Formation in the Transitional Landscape Zone: Weathering and Alteration of Parent Rocks. Journal of Environments, 5(1). DOI: 10.20448/journal.505.2018.51.1.7.

Purwaningsih R., Hartanti H., Hatta D., Ariyanti S., Putri H., Paradisa D., Dewi I., Priyawati E., Stakhis E., Salsabila G., Mashum H., Pulungan N. A., Handayani S., Sartohadi J., and Gomez C. (2025). Subsoil Mineralogy as Environmental Factors in Controlling Topsoil Material in the Menoreh–Sumbing Volcanic Structural Transitional Landscape, Central Java. Journal of Water and Land Development, 67 (X–XII): 73–85(67). DOI: 10.24425/jwld.2025.156041.

Purwaningsih R., Sartohadi J., and Anggri M. (2020). Trees and crops arrangement in the agroforestry system based on slope units to control landslide reactivation on volcanic foot slopes in Java, Indonesia. Land, 9(9). DOI: 10.3390/LAND9090327.

Ran Q., Hong Y., Li W., and Gao J. (2018). A modelling study of rainfall-induced shallow landslide mechanisms under different rainfall characteristics. Journal of Hydrology, 563. DOI: 10.1016/j.jhydrol.2018.06.040.

Samodra G., Ramadhan M. F., Sartohadi J., Setiawan M. A., Christanto N., and Sukmawijaya A. (2020). Characterization of displacement and internal structure of landslides from multitemporal UAV and ERT imaging. Landslides, 17(10). DOI: 10.1007/s10346-020-01428-0.

Sartohadi J., Rahma A. D., and Nugraha S. S. (2024). Productive conservation at the landslide prone area under the threat of rapid land cover changes. Open Geosciences, 16(1). DOI: 10.1515/GEO-2022-0700/MACHINEREADABLECITATION/RIS.

Schmittbuhl M., Allenbach B., Le Minor J. M., and Schaaf A. (2003). Elliptical descriptors: Some simplified morphometric parameters for the quantification of complex outlines. Mathematical Geology, 35(7). DOI: 10.1023/B: MATG.0000007783.72366.0c.

Segoni S., Ajin R. S., Nocentini N., and Fanti R. (2024). Insights gained from the review of landslide susceptibility assessment studies in Italy. REMOTE SENSING, 16(23), 1–31. DOI: 10.3390/RS16234491.

Shen W., Berti M., Li T., Benini A., and Qiao Z. (2022). The influence of slope gradient and gully channel on the run-out behavior of rockslide-debris flow: an analysis on the Verghereto landslide in Italy. Landslides, 19(4). DOI: 10.1007/s10346-022-01848-0.

Tarolli P., and Sofia G. (2016). Human topographic signatures and derived geomorphic processes across landscapes. Geomorphology, 255, 140–161. DOI: 10.1016/J.GEOMORPH.2015.12.007.

Taylor F. E., Malamud B. D., Witt A., & Guzzetti F. (2018). Landslide shape, ellipticity and length-to-width ratios. Earth Surface Processes and Landforms, 43(15). DOI: 10.1002/esp.4479.

Thorn C. E., and Welford M. R. (1994). The Equilibrium Concept in Geomorphology. Annals of the Association of American Geographers, 84(4), 666–696. DOI: 10.1111/J.1467-8306. 1994.TB01882. X.

Tort A. (2003). Elliptical Fourier functions as a morphological descriptor of the genus Stenosarina (Brachiopoda, Terebratulida, New Caledonia). Mathematical Geology, 35(7). DOI: 10.1023/B: MATG.0000007784.18452.73.

Trantham G. (2023). Improving Detail in Shaded Relief. Cartographic Perspectives, 2023(101). DOI: 10.14714/CP101.1789.

Vuillez C., Tonini M., Sudmeier-Rieux K., Devkota S., Derron M. H., and Jaboyedoff, M. (2018). Land use changes, landslides and roads in the Phewa Watershed, Western Nepal from 1979 to 2016. Applied Geography, 94. DOI: 10.1016/j.apgeog.2018.03.003.

Wida W. A., Maas, A., and Sartohadi J. (2019). Pedogenesis of Mt. Sumbing Volcanic Ash above The Alteration Clay Layer in The Formation of Landslide Susceptible Soils in Bompon Sub-Watershed. Ilmu Pertanian (Agricultural Science), 4(1). DOI: 10.22146/ipas.41893.

Wu Y. Bin, Duan Z., Peng J. B., and Zhang Q. (2024). Implications of sand grains' mobility and inundating area to landslides at different slope angles. Granular Matter, 26(1). DOI: 10.1007/s10035-023-01387-y.

Yin Z., Qin X., and Zhao W. (2014). Characteristics of Landslides from Sigou Gorge to Lagan Gorge in the Upper Reaches of Yellow River. In Landslide Science for a Safer Geoenvironment (Vol. 1). DOI: 10.1007/978-3-319-04999-1_56.